Supplementary Information for

Versatile pH-response Micelles with High Cell-Penetrating Helical Diblock Copolymers for Photoacoustic Imaging Guided Synergistic Chemo-Photothermal Therapy

Shengyu Shi, Yajing Liu, Yu Chen, Zhihuang Zhang, Yunsheng Ding, Zongquan Wu, Jun Yin*, and Liming Nie*

S. Y. Shi, Z. P. Yu, Z. H. Zhang, Prof. Y. S. Ding, Prof. J. Yin, Prof. Z. Q. Wu

Department of Polymer Science and Engineering, School of Chemistry and Chemical Engineering, Hefei University of Technology and Anhui Key Laboratory of Advanced Functional Materials and Devices, Hefei, 230009, China.

E-mail: yinjun@hfut.edu.cn

Dr. Y. Liu, Prof. L. Nie

State Key Laboratory of Molecular Vaccinology and Molecular Diagnostics & Center for Molecular Imaging and Translational Medicine, School of Public Health, Xiamen University, Xiamen, 361102, China.

E-mail: nielm@xmu.edu.cn

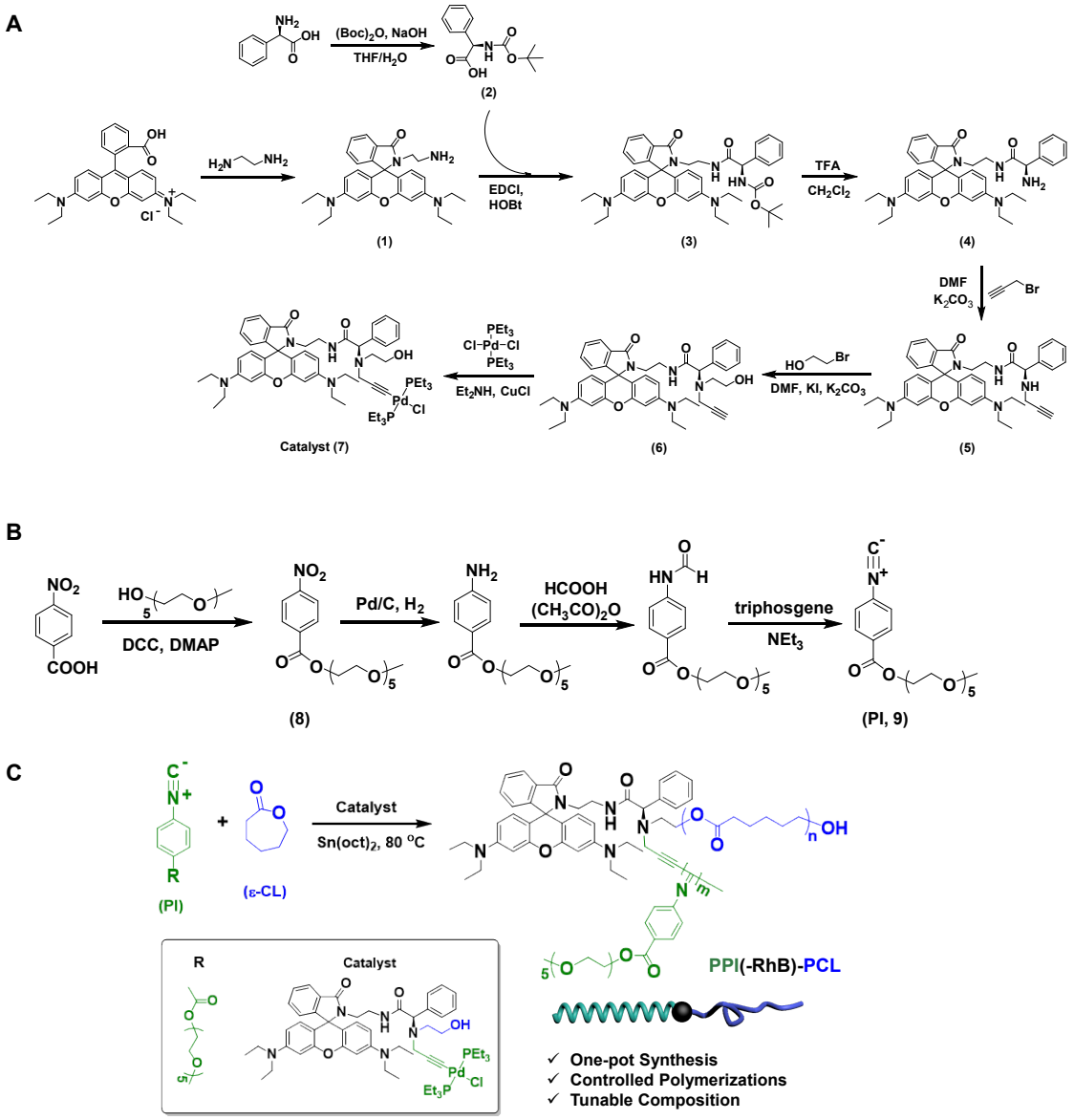

Scheme S1. Synthetic routes employed for the preparation of (A) bifunctional catalyst, $ClPd(PEt_3)_2$-RhB-OH, (B) PI, and (C) the "one-pot" copolymerization of PEGylated phenyl isocyanide monomers (PI; 9) and ε-caprolactone (ε-CL) by two mechanistically distinctive living polymerizations with $ClPd(PEt_3)_2$-RhB-OH as an initiator.

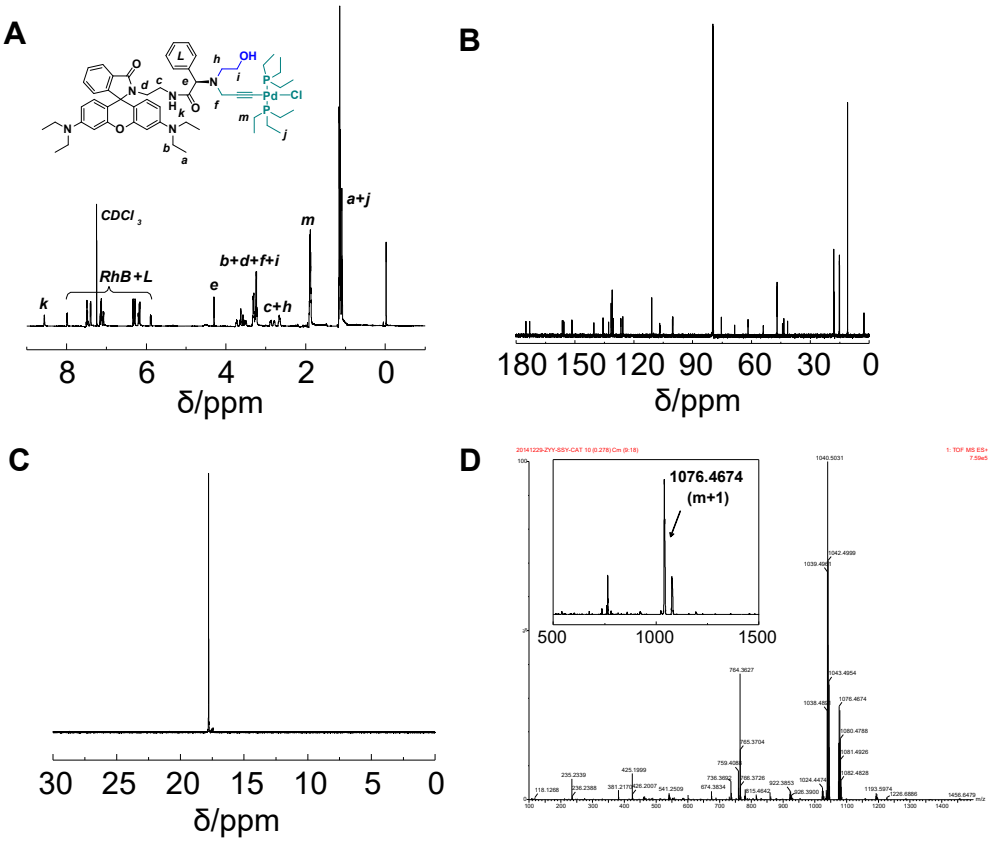

Figure S1. (A) ^{1}H, (B) ^{13}C, (C) ^{31}P NMR (600 MHz, $CDCl_3$, 25 ℃), (D) mass spectra and obtained for the bifunctional catalyst $ClPd(PEt_3)_2$-RhB-OH.

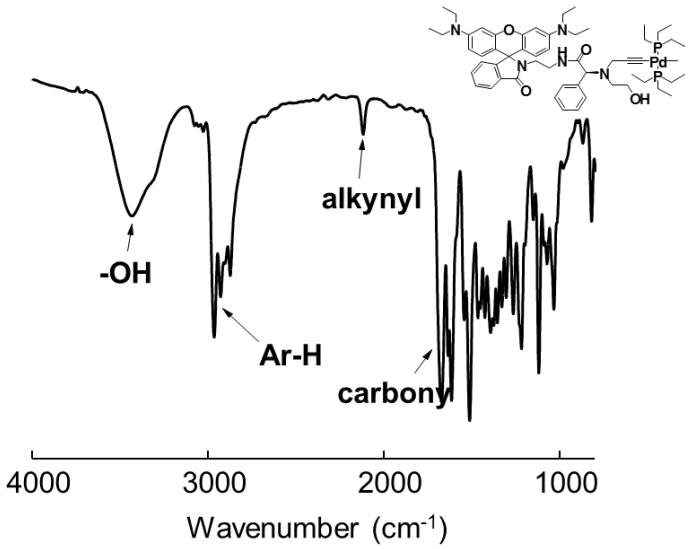

Figure S2 FT-IR spectrum of palladium(II) modified complex (7) measured at 25 ℃ using KBr pellets.

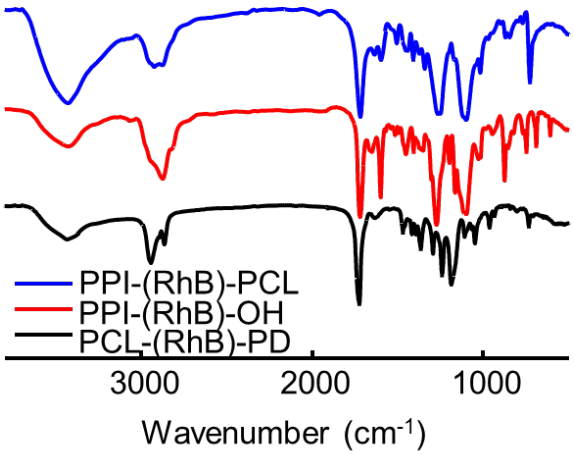

Figure S3. FT-IR spectra of PCL(-RhB)-Pd(PEt_3)$_2$Cl, PPI(-RhB)-OH, and PPI(-RhB)-PCL measured at 25 ℃ using KBr pellets.

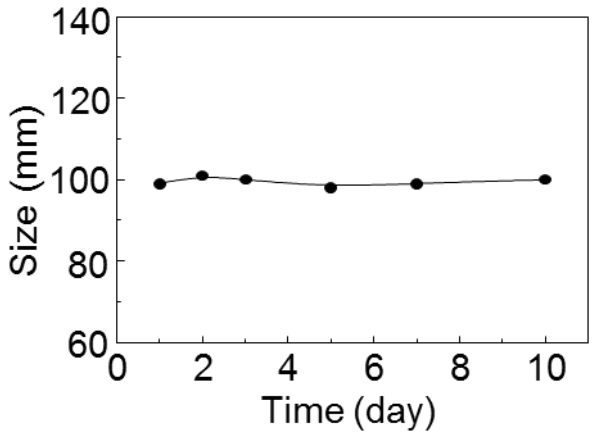

Figure S4. Size variation of ICM in water at 25 ℃ during 10 days of storage.

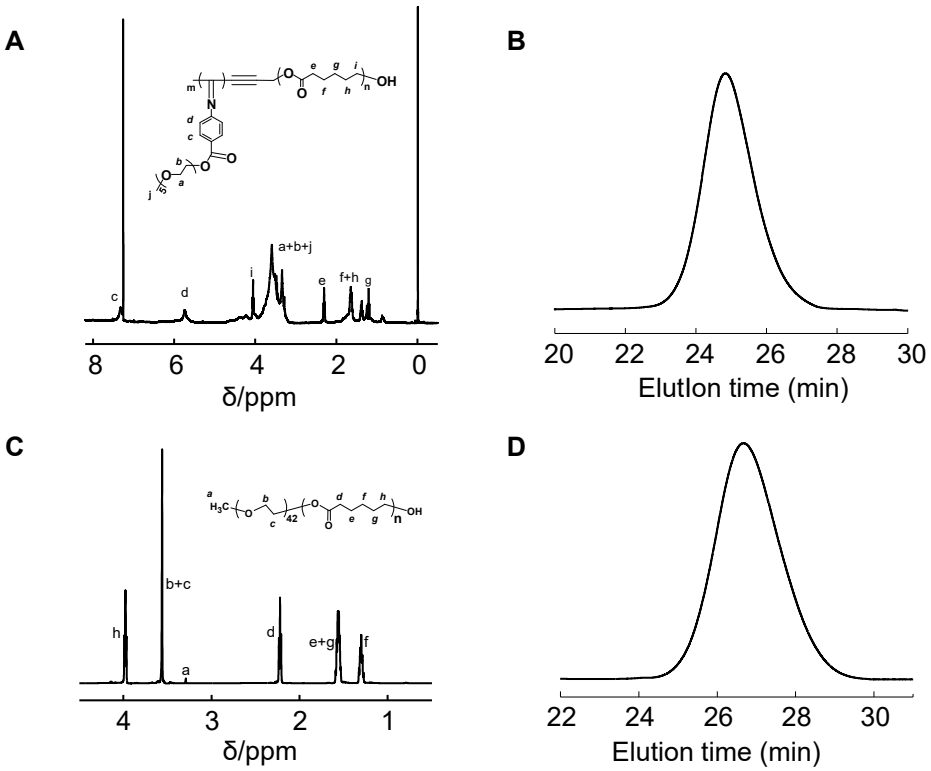

Figure S5. (A) ^{1}H NMR spectrum of PPI-PCL measured in $CDCl_3$ at 25 ℃ (600 MHz). (B) SEC trace obtained for PPI-PCL, using THF as eluent. (C) ^{1}H NMR spectrum of mPEG-PCL measured in $CDCl_3$ at 25 ℃ (600 MHz). (D) SEC trace obtained for mPEG-PCL, using THF as eluent.

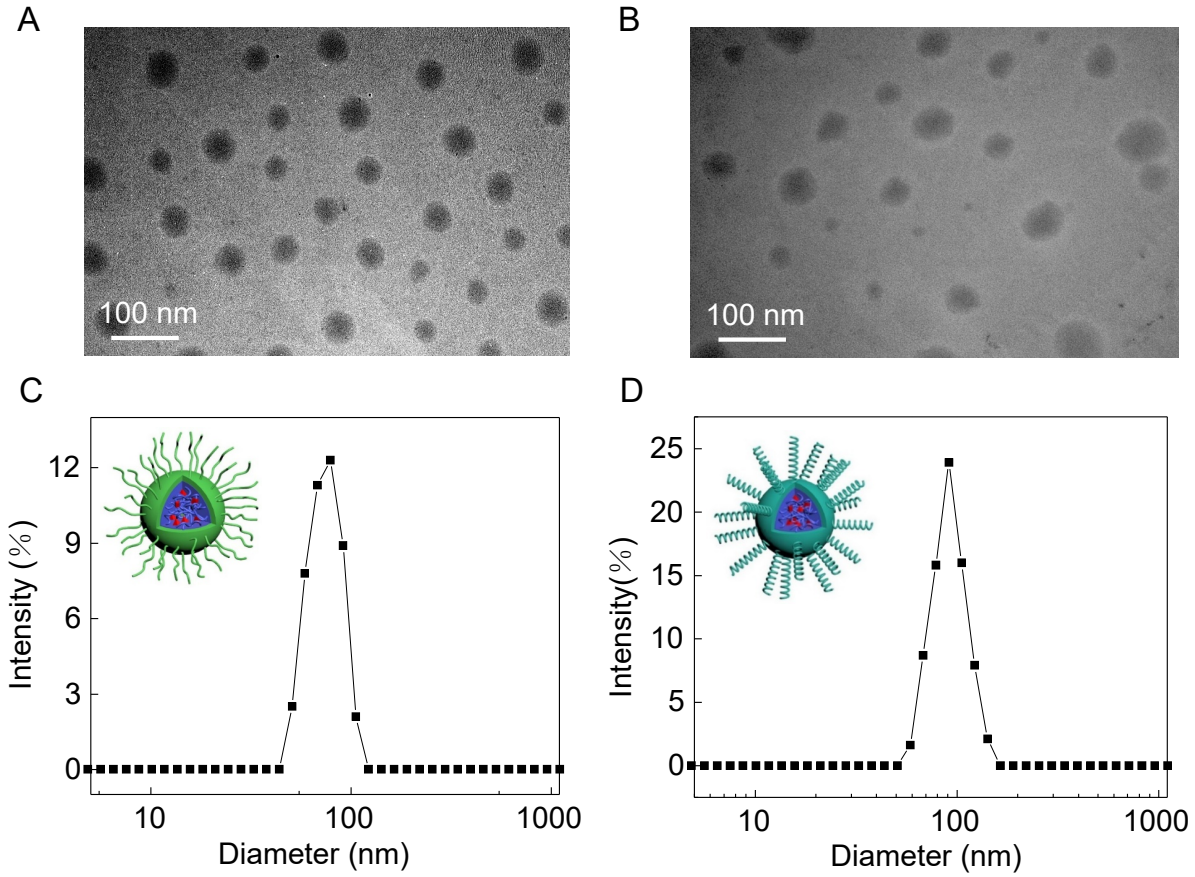

Figure S6. TEM images observed for (A) Nile red@mPEG-PCL and (B) Nile red@PPI-PCL micelles dried from aqueous dispersions. DLS spectra obtained for (C) Nile red@mPEG-PCL and (D) Nile red@PPI-PCL micelles in water. All the concentration were fixed at 0.5 g/L.

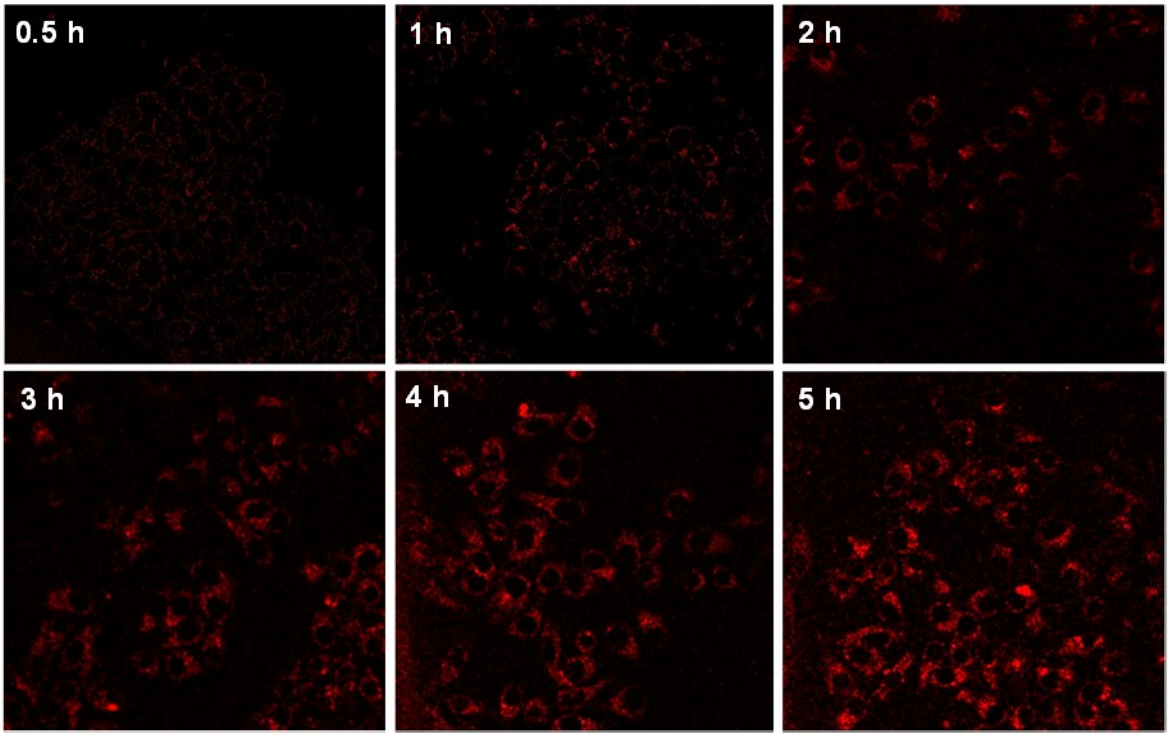

Figure S7. Incubation duration-dependent CLSM images of live HeLa cells when culturing at 37 ℃ with ICM (1.0 g/L). The red channel was excited at 543 nm and collected between 555 and 600 nm.

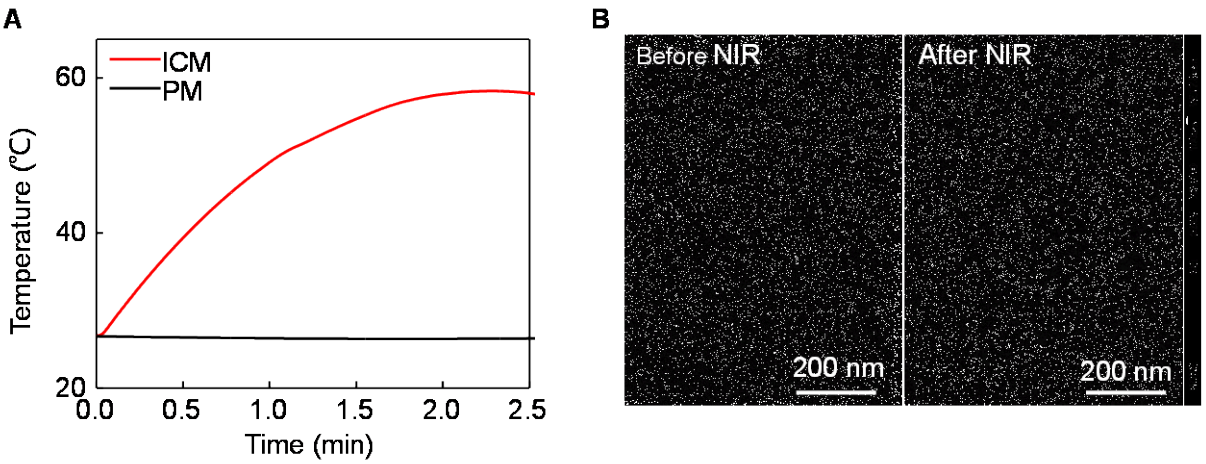

Figure S8. (A) Temperature change of ICM and PM as a function of irradiation time. Both of the concentrations were fixed at 1.0 g/L. (B) SEM images observed for the morphologies of ICM before and 10 min after NIR irradiation.

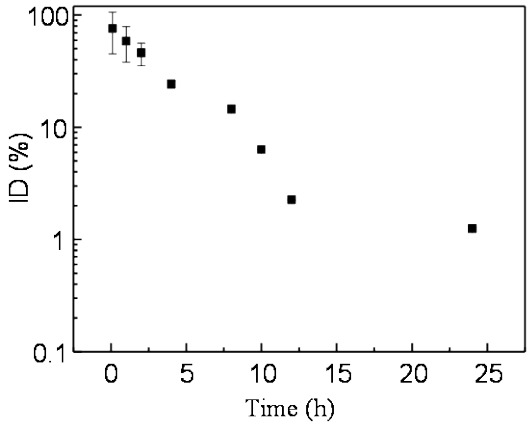

Figure S9. Plasma drug concentration versus time after intravenous injection of ICM

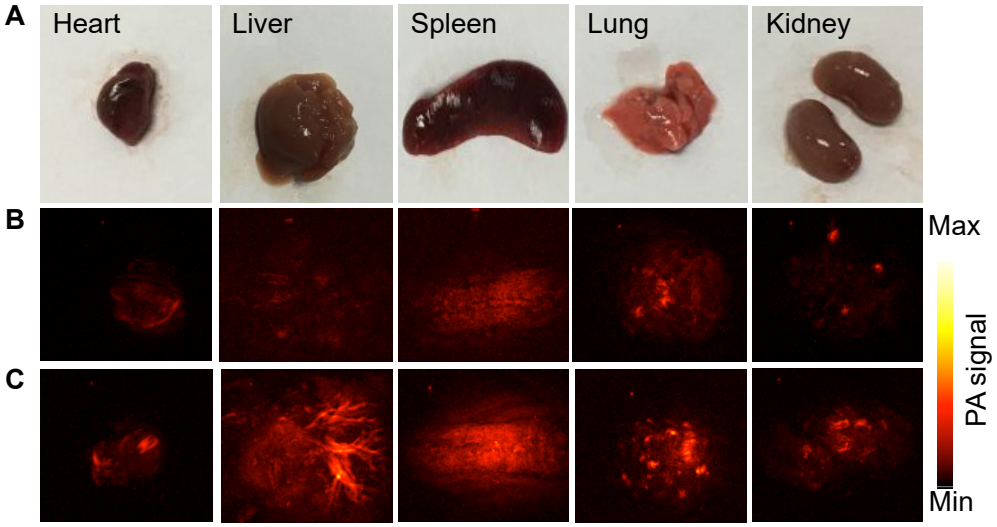

Figure S10. *Ex vivo* PA imaging of the main mouse organs before and 24 h after intravenous injection of ICM. (A) Photographs of main mouse organs (heart, liver, spleen, lung, kidney). PA images of main mouse tissues (B) before and (C) 24 h after intravenous injection of ICM.

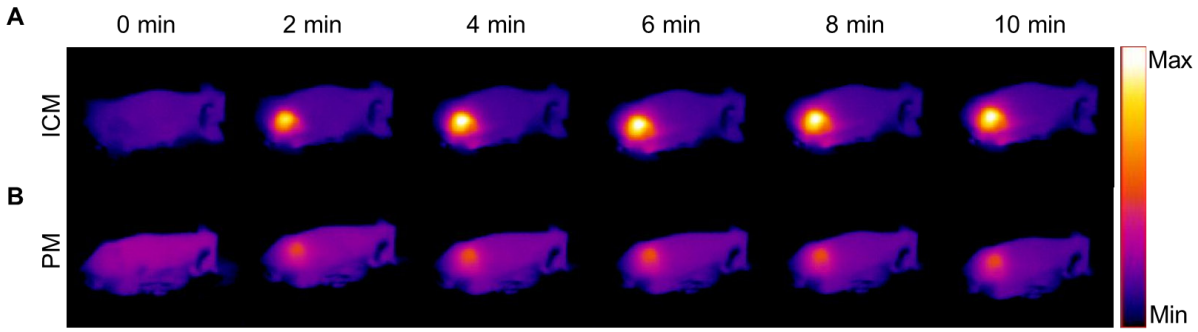

Figure S11. *In vivo* NIR thermal images obtained 24 h after intravenous injection of (A) ICM or (B) PM into mice and irradiated by 808 nm laser at power density of 1 W cm^{-2} as a function of irradiation time.

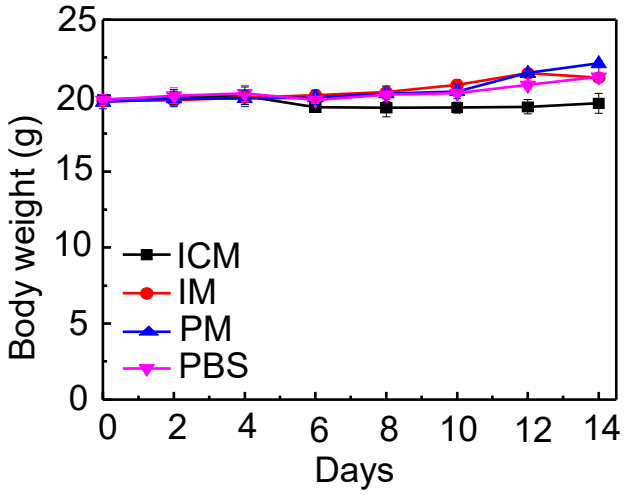

Figure S12. Body weight curves of tumor-bearing mice after 808 nm laser irradiation.

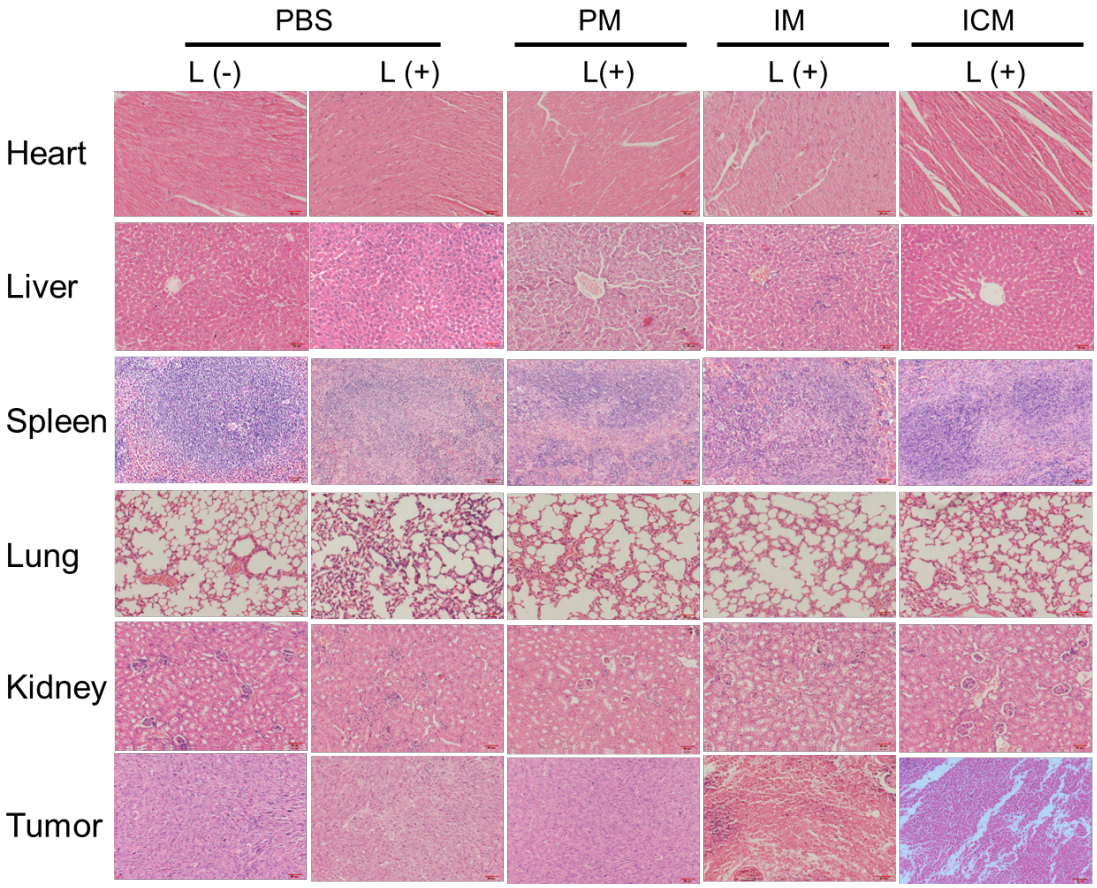

Figure S13. Hematoxylin and eosin (H&E)-stained slices of the heart, liver, spleen, lung, kidney, and tumor in mouse after treated by 808 nm laser at power density of 1 W cm^{-2} for 10 min.